Modelling Common Dynamics in Multichannel Signals with Applications to Artifact and Background Removal in EEG Recordings

Wim De Clercq, Bart Vanrumste, *Member, IEEE,*
Jean-Michel Papy, Wim Van Paesschen*, and Sabine Van Huffel, *Senior Member, IEEE*

Abstract

Removing artifacts and background EEG from multichannel interictal and ictal EEG has become a major research topic in EEG signal processing in recent years. We applied for this purpose a recently developed subspace-based method for modelling the common dynamics in multichannel signals. When the epileptiform activity is common in the majority of channels and the artifacts appear only in a few channels the proposed method can be used to remove the latter. The performance of the method was tested on simulated data for different noise levels. For high noise levels the method was still able to identify the common dynamics. In addition, the method was applied to a real life EEG recording containing interictal activity contaminated with muscle artifact. The muscle artifacts were removed successfully. For both the synthetic data and the analyzed interictal activity the results were compared with the results obtained with principle component analysis (PCA). In both cases the proposed method performed better than PCA.

W. De Clercq is a research assistant of the Fund for Scientific Research-Flanders (Belgium) (FWO-Vlaanderen). Dr. Sabine Van Huffel is a full professor at the Katholieke Universiteit Leuven, Belgium. B. Vanrumste is a postdoctoral fellow at the Katholieke Universiteit Leuven in Belgium. Currently he is funded by the Programmatorische Federale Overheidsdienst Wetenschapsbeleid of the Belgian Government. Research is supported by Research Council KUL: GOA-Mefisto 666, IDO /99/003 and /02/009 (Predictive computer models for medical classification problems using patient data and expert knowledge), several PhD/postdoc and fellow grants; Flemish Government: FWO: PhD/postdoc grants, projects, G.0078.01 (structured matrices), G.0407.02 (support vector machines), G.0269.02 (magnetic resonance spectroscopic imaging), G.0270.02 (nonlinear Lp approximation), research communities (ICCoS, ANMMM); IWT: PhD Grants; Belgian Federal Science Policy Office IUAP P5/22 (‘Dynamical Systems and Control: Computation, Identification and Modelling’); EU: PDT-COIL, BIOPATTERN, ETUMOUR.

W. De Clercq, J.-M. Papy, B. Vanrumste and S. Van Huffel are with the Department of Electrical Engineering ESAT-SCD(SISTA), Katholieke Universiteit Leuven, Leuven, Belgium.

*W. Van Paesschen is with the Department of Neurology, University Hospital Gasthuisberg, Leuven, Belgium.

Index Terms

Common dynamics, artifact removal, background EEG removal, ictal and interictal EEG, singular value decomposition, subspace based, exponentially damped sinusoids.

Modelling Common Dynamics in Multichannel Signals with Applications to Artifact and Background Removal in EEG Recordings

I. Introduction

Electroencephalography (EEG) measures the electric potentials on the skull and provides a continuous measure of cortical function with excellent time resolution. It is a tool to study the brain dynamics non-invasively. Typical waveforms appear in the EEG of patients with epilepsy. Ictal EEG (activity during a seizure) and interictal events (epileptic activity between seizures) can be distinguished. This activity can be identified on the majority of the EEG electrodes if the underlying electrical sources (the epileptogenic region) are located in deeper cortical structures as in Mesial Temporal Lobe Epilepsy (MTLE) [1]. In reality noise is added to this EEG obscuring the brain function of interest and making the interpretation of the EEG less straightforward. Some typical contributors are the heart, muscle and eye-movement artifacts. In general, these artifacts appear on a limited number of channels in EEG recordings. Apart from these electrical active tissues, many brain areas other than the epileptogenic region are active too. The EEG generated by these areas is often called background EEG.

Many methods exist in the literature which attempt to remove or attenuate artifacts and background EEG from the multichannel interictal and ictal EEG. Among them are broadband filtering methods, regression methods, and component based methods such as principal component analysis (PCA) and independent component analysis (ICA) [2]–[7].

In this paper we introduce a new approach towards removing artifacts and background EEG. A new subspace based method is used to model the common dynamics in a multichannel recording [8]. With common dynamics we mean the same waveform appearing over multiple channels. This common waveform can have a different amplitude and phase for each channel. The proposed method can be exploited to remove artifacts when epileptiform activity appears in the majority of channels and the artifacts only in few. Since the spatial correlation of the background EEG is low [9], the background EEG will also be removed by applying this method.

The paper is organized as follows. In section II the subspace based method for modelling the common dynamics in a multichannel recording is described. A simulation study is presented in section III where the method is applied to simulated data with known underlying common dynamics in order to test the performance of the method. As proof of concept, section IV shows the results obtained when applying the method to a real life multichannel EEG recording with the aim of modelling the common dynamics along the different electrodes and thereby removing the artifacts and background EEG not related to the epileptiform activity. In both sections, the results are compared with results obtained with PCA decomposition of the EEG. Finally, in sections V and VI our findings are discussed and suggestions for further work are given.

II. METHODS

First the Exponentially Damped Sinusoidal (EDS) [10] model will be introduced. This model provides an appropriate framework to describe the common dynamics in a given set of signals. Next, the proposed method for modelling the common dynamics will be explained.

A. EDS model

A way to analyze EEG signals is to quantify them directly in the time domain by means of model-based (or parametric) methods. We used the parametric EDS model where the signal is modelled as a finite sum of K discrete-time exponentially damped complex sinusoids:

$$\begin{aligned} x(n) &= \sum_{k=1}^{K} a_k \exp(j\phi_k) \exp\left((-d_k + j2\pi f_k) n\Delta t\right) + e(n), \\ n &= 0, 1, \ldots, N-1; \end{aligned} \tag{1}$$

where $j = \sqrt{-1}$, $n\Delta t$ is the time lapse between the origin and the sample $x(n)$, Δt is the sampling interval, and $e(n)$ is white gaussian noise. The parameters of this model are the amplitudes a_k, the phases ϕ_k, the damping factors d_k and the frequencies f_k. The model function (1) can be rewritten in terms of complex amplitudes $c_k = a_k \exp(j\phi_k)$ and signal poles $z_k = \exp\left((-d_k + j2\pi f_k)\Delta t\right)$ as follows

$$\begin{aligned} x(n) &= \sum_{k=1}^{K} c_k z_k^n + e(n), \\ n &= 0, 1, \ldots, N-1. \end{aligned} \tag{2}$$

Since exponentially damped sinusoids are a set of basis functions, they can be used to model any arbitrary signal sufficiently closely provided the model order is high enough. The EDS model can be extended to

real-valued signals since any real-valued sinusoid can be expressed as a superposition of two complex sinusoids. Consequently, the model order K is equal to twice the number of sinusoids that comprise the real-valued signal.

B. Common dynamics

It is often of great interest to extract the common information present in a given set of signals or multichannel recording. This is possible by going to the subspace representation of the signals and capturing the subspace common to all signals. In this section we introduce a new method which allows determining this common subspace [8]. The method can be divided into two parts; in the first part each channel is preprocessed separately by selecting the signal subspace of interest as explained in section II-B.2. This preprocessing step facilitates capturing the common subspace. The second part determines the common subspace and the parameters of the common signal poles as shown in section II-B.3. Before explaining our method the mathematical problem formulation is given.

1) Problem formulation: Given S channels $x_s(n),\ s = 1, \ldots, S;\ n = 0, \ldots, N-1$ which can be modelled as a sum of exponentially damped sinusoids. Let those S channels have K_c common poles $z_k,\ k = 1, \ldots, K_c$:

$$\begin{aligned} x_1(n) &= \sum_{k=1}^{K_1-K_c} c'_{1,k} z_{1,k}^n + \sum_{k=1}^{K_c} c_{1,k} z_k^n + e_1(n), \\ &\vdots \\ x_s(n) &= \sum_{k=1}^{K_s-K_c} c'_{s,k} z_{s,k}^n + \sum_{k=1}^{K_c} c_{s,k} z_k^n + e_s(n), \\ &\vdots \\ x_S(n) &= \sum_{k=1}^{K_S-K_c} c'_{S,k} z_{S,k}^n + \sum_{k=1}^{K_c} c_{S,k} z_k^n + e_S(n), \end{aligned} \tag{3}$$

with $z_{s,k},\ k = 1, \ldots, (K_s - K_c)$ the remaining signal poles at channel s. The common dynamics are described by the common signal poles. The corresponding amplitudes and phases can differ from channel to channel.

2) Algorithm part 1 (Single-channel preprocessing): In this section each channel is preprocessed separately. This is done by going to a subspace representation of the channel and selecting the subspace

of interest. The selected signal subspace serves as an input of section II-B.3. The preprocessing is summarized as follows:

- **input:** S channels consisting of the data points $x_s(n),\ n = 0, \ldots, N-1;\ s = 1, \ldots, S.$; individual model order K_s for each channel s.
- **output:** a basis $U_{s_{K_s}}$ of the signal subspace of each channel $s = 1, \ldots, S$ and the preprocessed data points $x'_s(n)$.
- ***Step 1***. For every channel $s, s = 1, \ldots, S$ arrange the data points $x_s(n), n = 0, \ldots, N-1$ in a Hankel matrix H_s of dimensions $L \times M$ as follows:

$$H(x_s) = H_s = \begin{bmatrix} x_s(0) & x_s(1) & x_s(2) & \cdots & x_s(M-1) \\ x_s(1) & x_s(2) & \ddots & \cdots & \vdots \\ x_s(2) & \ddots & \ddots & \cdots & \vdots \\ \vdots & \vdots & \vdots & \vdots & x_s(N-2) \\ x_s(L-1) & \cdots & \cdots & x_s(N-2) & x_s(N-1) \end{bmatrix}, \tag{4}$$

  where N=L+M-1.

- ***Step 2***. Compute the Singular Value Decomposition (SVD) [11], [12] of each Hankel matrix H_s:

$$H_s = U_s \Sigma_s V_s^H, \tag{5}$$

  where the superscript H denotes the hermitian conjugate. According to [13], in the absence of noise the SVD of H_s reduces to the product

$$H_{s_{K_s}} = U_{s_{K_s}} \Sigma_{s_{K_s}} V_{s_{K_s}}^H, \tag{6}$$

  where $U_{s_{K_s}}$, $V_{s_{K_s}}$ are respectively the first K_s columns of U_s, V_s and $\Sigma_{s_{K_s}}$ is the leading $(K_s \times K_s)$ submatrix of Σ_s. In the presence of noise H_s is full rank. In this case, the truncated SVD, $H_{s_{K_s}}$, of H_s is the best rank-K_s approximation of H_s and the column vectors of the truncated matrix $U_{s_{K_s}}$ span the signal subspace [13]. This matrix will serve as an input of section II-B.3. By averaging the anti-diagonals of the truncated matrix $H_{s_{K_s}}$ we can recover the Hankel structure and extract the filtered time series $x'_s(n)$ [14], i.e.

$$x'_s(n) \ = \ \frac{1}{a} \sum_{i+j=n+2} H_{s_{K_s}}(i,j), \tag{7}$$

  with $a = (n+1)$ for $n = 0, \ldots, M-1$ and $a = (N-n)$ for $n = M, \ldots, N-1$.

In practice the number of sinusoids present in a given signal and thus the corresponding model order K_s is not known a priori. Therefore, we introduce the following rule for truncating the U_s matrices in step 3. The U_s matrices are truncated when:

$$\begin{cases} \sigma_s^2(K_s) & \geq \ d \cdot \sigma_s^2(1) \\ \sigma_s^2(K_s+1) & < \ d \cdot \sigma_s^2(1) \end{cases} \tag{8}$$

with $\sigma_s(k)$ the k^{th} largest singular value corresponding to the k^{th} left singular vector in U_s. The parameter d, which can be defined by the user, determines which left singular vectors belong to the signal subspace. As such, the individual model orders K_s are replaced by d at the input of algorithm part 1.

3) Algorithm part 2 (Common dynamics extraction): First it is shown how to estimate the number of common signal poles and select the common subspace of a given set of signals. Once the common subspace is selected the parameters of the common poles are estimated in the second step. Finally, the corresponding estimates for the amplitudes and phase of the common signal poles are determined for each channel separately. The algorithm is summarized as follows:

- **input:** a basis $U_{s_{K_s}}$ of the signal subspace of each channel $s = 1, \ldots, S$ and the preprocessed data points $x'_s(n)$.
- **output:** the estimate of the parameters $d_k,\ f_k,\ k = 1, \ldots, K_c$ of the common signal poles and the corresponding amplitudes and phases $a_{s,k},\ \phi_{s,k};\ k = 1, \ldots, K_c,\ s = 1, \ldots, S$.
- ***Step 1***. Stack the truncated $U_{s_{K_s}}$, $s = 1, \ldots, S$ matrices into a $L \times \sum_{s=1}^{S} K_s$ matrix

$$U_{stacked} = [U_{1_{K_1}} | U_{2_{K_2}} | \ldots | U_{S_{K_S}}]. \tag{9}$$

  and compute the SVD of this resulting matrix

$$U_{stacked} = U_c \Sigma_c V_c^H. \tag{10}$$

  In [8] it is explained why the SVD of $U_{stacked}$ directly gives information about the number of common poles and the common subspace spanned. Assuming that there are K_c poles common to S signals, the diagonal core matrix Σ_c contains a first set of K_c values equal to $\sqrt{S}$. The K_c first vectors of the left singular vector matrix $U_{c_{K_c}}$ span the common subspace related to the common signal poles. We select these vectors by truncating U_c to a matrix of rank K_c, $U_{c_{K_c}}$.

- ***Step 2***. Form the following overdetermined set of linear equations

$$U^{\uparrow}_{c_{K_c}} \approx U_{c_{K_c}\downarrow} Z, \tag{11}$$

where the arrows $\uparrow$ and $\downarrow$ denote the last and first row-deleting operator respectively. The Total Least Squares (TLS) solution of this set of equations is given by:

$$\tilde{Z} = -W_{12}W_{22}^{-1}, \tag{12}$$

where

$$W = \begin{bmatrix} W_{11_{K_c \times K_c}} & W_{12_{K_c \times K_c}} \\ W_{21_{K_c \times K_c}} & W_{22_{K_c \times K_c}} \end{bmatrix}, \tag{13}$$

is obtained from the SVD of the matrix $[U^{\uparrow}_{c_{K_c}} U^{\downarrow}_{c_{K_c}}]$:

$$[U^{\uparrow}_{c_{K_c}} U^{\downarrow}_{c_{K_c}}] = Y_{(L-1)\times(L-1)} \Gamma W^{H}_{2K_c \times 2K_c}. \tag{14}$$

Once $\tilde{Z}$ is estimated, its K_c eigenvalues λ_k give an estimate of the common signal poles [13]:

$$\lambda_k = \hat{z}_k = \exp\{(-\hat{d}_k + j2\pi\hat{f}_k)\Delta t\}, k = 1, \ldots, K_c. \tag{15}$$

From these signal poles, frequencies and dampings are easily calculated.

- ***Step 3***. The corresponding estimates for amplitudes $a_{s,k}$ and phases $\phi_{s,k}$, $s = 1, \ldots, S; k = 1, \ldots, K_c$ of the common signal poles are determined for each channel separately by filling in the obtained signal poles in the model function (3) and solving the resulting equations

$$x'_s(n) \approx \sum_{k=1}^{K_c} c_{s,k}\hat{z}_k^n, n = 0, 1, \ldots, N-1. \tag{16}$$

The $x_s(n)$ in (3) are replaced by the preprocessed $x'_s(n)$ of (7) for a better estimation of the amplitudes and phases.

III. Simulation study

Simulations are carried out to test the performance of the proposed method for different noise levels.

A. Simulation

Consider a matrix X of dimension 250-by-19 representing a 19 channel EEG section of 1.0 s long. Each column vector $X_s, s = 1, \ldots, 19$ of X contains the time course of an EEG channel and corresponds to the $x_s(n)$ mentioned above:

$$X = [X_1, X_2, \ldots, X_{19}], \tag{17}$$

$$X_s = [x_s(0), x_s(1), \ldots, x_s(249)]^T, \tag{18}$$

with $s = 1, \ldots, 19$. In this simulation study X includes both seizure activity, and superimposed noise. Both signals are described below.

1) Seizure activity: The EEG of the ictal activity was generated using a fixed dipole in a three-shell spherical head model with a moment having a 4 Hz sinusoidal waveform (for example typical in patients with MTLE [1]). The amplification factors at each electrode were computed by solving the forward problem for a dipole in a three-shell spherical head model consisting of a brain, a skull and a scalp compartment [15]. Each compartment had a specific conductivity with a ratio equal to 1:1/16:1 for the brain, skull and scalp compartment respectively [16]. The brain and scalp conductivity was $3.3 \times 10^{-4}/\Omega mm$ [17]. Radii of the outer boundary of the brain, skull and scalp region equal to respectivly 8 cm, 8.5 cm and 9.2 cm were used. The dipole coordinates x (left ear to right ear), y (posterior to anterior) and z (up, through the Cz electrode) were $(0.5,\ 0,\ 0.1)$ relative to the outer radius and the dipole orientations $d_x,\ d_y$ and d_z were equal to (1, 0, 0). The amplification factors at each electrode were then multiplied with a 4Hz sine wave. 19 electrodes were used: Fp2, F8, T4, T6, O2, F4, C4, P4, Fz, Cz, Pz, Fp1, F7, T3, T5, O1, F3, C3 and P3 placed according to the 10-20 system for electrode placement [18]. The time course of the scalp potentials was stored in a 250-by-19 dimensional matrix A and is shown in Fig. 1(a).

2) Noise: Let B denote a 250-by-19 noise matrix representing awake background EEG activity from a normal subject, 50 Hz line noise, and muscle artifact. The 50 Hz line noise was superimposed on the background EEG on electrodes O1 and P3 and was simulated by a 50 Hz sinusoid waveform sampled at 250 Hz. The muscle artifact was simulated by filtering white gaussian noise with a band pass filter between 15 and 30 Hz. The simulated muscle artifact was superimposed on the background EEG on channels F8 and Cz. The amplitudes of the muscle artifact and 50Hz noise signal were chosen in a realistic way. The noise matrix is shown in Fig. 1(b). Because the spatial correlation of the background EEG is low, no common waveform appears on all channels of B.

3) The simulated signal: In the simulation study the noise matrix B is superimposed on the signal matrix A containing the common dynamics:

$$X(\lambda) = A + \lambda \cdot B, \tag{19}$$

with $\lambda \in \mathbb{R}$. The Root Mean Squared (RMS) value of the signal is then equal to

$$RMS(A) = \sqrt{\frac{1}{S \cdot N} \sum_{s=1}^{S} \sum_{n=0}^{N-1} A_s^2(n)}, \tag{20}$$

and the RMS value of the noise is equal to

$$RMS(\lambda \cdot B) = \sqrt{\frac{1}{S \cdot N} \sum_{s=1}^{S} \sum_{n=0}^{N-1} (\lambda \cdot B_s^2(n))}. \tag{21}$$

An important measure is the noise level (nl) which is defined as follows,

$$nl = \frac{RMS(A)}{RMS(\lambda \cdot B)}. \tag{22}$$

Changing the λ parameter alters the noise level of our simulated signal.

B. Results of simulation study

1) Aim of the simulation study: The aim of this simulation study was to evaluate the performance of the proposed method in modelling the common dynamics, the 4Hz epileptiform activity, for different noise levels. We performed several simulations with different noise levels. The performance is expressed in terms of the Relative Root Mean Squared Error (RRMSE):

$$RRMSE = \frac{RMS(A - \hat{A})}{RMS(A)} \cdot 100[\%], \tag{23}$$

where $\hat{A}$ is an estimate of the common dynamics.

2) Results: Fig. 2(a) shows a simulation data matrix X under study with a noise level equal to 0.95. This set of signals was processed with the following parameters: $N = 250$, $L = 126$, $M = 125$. The U_s matrices are truncated according to (8) with d equal to 0.1. Fig. 2(c) shows the EEG signals after preprocessing the channels separately based on this truncation and section II-B.2. The background activity is reduced for each channel. For channels F8 and Cz the muscle activity is still present as it is the dominant activity for those channels. Also the 50 Hz line noise is still present in channels O1 and P3 after preprocessing.

Fig. 3 shows the resulting squared singular values σ_c^2 of the stacked matrix $U_{stacked}$ (10). There are two squared singular values close to 19, indicating that there are two common signal poles in all 19 channels. The reconstructed EEG based on these two signal poles according to step 2 and 3 in section II-B.3 had an RRMSE of 13% and is shown in Fig. 2(d). By modelling the common dynamics in the 19

channels the remaining noise after preprocessing was successfully removed.

For comparison, we applied SVD directly to the data matrix X to derive the principal components of the simulated EEG signal (= PCA) [4]. The $(N \times S)$ matrix X is then decomposed as a product of three matrices:

$$X = U\Sigma V^T, \tag{24}$$

where U is an $(N \times S)$ matrix containing the S normalized component waveforms that are decorrelated linearly and can be remixed to reconstruct the original EEG. The first principal component contained the 4 Hz epileptiform waveform and was selected. The reconstructed EEG based on this truncation had an RRMSE of 34% and is shown in Fig. 2(e).

The RRMSE as a function of the noise level is shown in Fig. 4. In this figure a comparison is made between the proposed method and PCA. For a noise level higher than 1.82 the background activity is too dominant on channel O2 compared to the epileptiform activity and the EDS model does not estimate the signal pole related to the epileptic activity in this channel. As a result the first squared singular values σ_c^2 of $U_{stacked}$ drop to 18. We stopped our simulation at this noise level. However, one could still continue by selecting the signal poles close to 18. The estimate of the common dynamics in channel O2 will then be equal to zero.

IV. Method applied to interictal activity

Fig. 5 shows a 10 s epoch of 19 channel scalp EEG recorded from a long-term Epilepsy Monitoring Unit. The electrodes are placed according to the 10-20 electrode placement system [18]. The sampling frequency is 250 Hz and an average reference is used. This EEG epoch contains several epileptic spikes. Channels O1 and F3 are contaminated with muscle artifact which obscures the epileptic spike activity on those channels. The EEG between the two vertical lines containing the epileptic spike is used for further analysis and is enlarged in Fig. 6(a). By determining the common dynamics present in all channels we wanted to enhance the spike activity and remove the artifact from channels O1 and F3. The following parameters were applied: $N = 70$, $L = 36$, $M = 35$. The U_s matrices are truncated according to (8) with d equal to 0.01. Fig. 6(b) shows the EEG signals after preprocessing the channels based on this truncation. For channels O1 and F3 the muscle artifacts can still be observed. For these channels the artifact is the dominant activity which can not be removed by the preprocessing part only.

Fig. 7 shows the resulting squared singular values σ_c^2 of the stacked matrix $U_{stacked}$ (10). There are four squared singular values close to 19, indicating that there are four common signal poles in all 19 channels. The reconstructed EEG based on these common signal poles according to step 2 and 3 in section II-B.3 is shown in Fig. 6(c). The muscle artifact is removed successfully on channels O1 and F3.

For comparison, Fig. 6(d) shows the result of the noise removal based on the truncated SVD of the data matrix. Hereby, the first principal component is selected for reconstruction.

V. DISCUSSION

In this paper, we introduced a new method for modelling the common dynamics in a multichannel recording. We showed that this method can be used to remove artifacts and background EEG from epileptiform EEG when the artifacts are distributed over less channels than the epileptiform activity. Since the spatial correlation of the background EEG is low, the background EEG is also reduced by the method.

The algorithm is divided into two parts. First each channel is preprocessed separately to select the subspace of interest. Here the parameter d determines the threshold between the signal and noise subspace. Truncating at a low value of d will not remove all the noise from each channel. Truncating at a high value of d has the danger of removing the signal poles modelling the common dynamics. In the second part of the algorithm the common signal poles are determined. Here all the signal poles not belonging to all channels are removed. It has the advantage that it also removes the signal poles that are more energetic than the signal poles representing the common dynamics (for example the muscle artifact is more energetic than the epileptiform activity on channels O1 and F3 in Fig. 6). These poles could never be removed by the preprocessing step only. Moreover, the truncation parameter d in the preprocessing step becomes less critical when applying the second part of the algorithm. The signal poles representing the noise that are not removed by the preprocessing step will be removed in the second part of the algorithm. However, putting d too low in the preprocessing part will lead to a less accurate estimate of the amplitudes and the phases of the common signal poles in the second part (cfr. (16)).

It is important to notice that the proposed method can be used on any multichannel EEG recording starting from 2 to N channels. One is not obliged to use the method on all recorded EEG channels. The

method can be used on a selection of EEG channels of interest to look for the common dynamics within the selected channels (for example, if a lateralization of the epileptic focus is a priori known).

As explained in section II-B.2, the first part of the algorithm preprocesses each channel separately by selecting the signal subspace of interest. The data points are arranged in a Hankel matrix and the SVD of this matrix is computed. The selection of the signal subspace is automated based on the energy of the components (8). This proposed method for the selection of the channel subspace is not unique. In [19] the selection of the channel subspace is done by applying ICA on a Hankel matrix. The advantage of the ICA-based method is that a better selection of the channel subspace is possible compared to SVD. However, we have shown that the preprocessing part of the algorithm must not be optimal since the remaining noisy components are removed by the second part of the algorithm as discussed above. Moreover, the obtained components after applying ICA are not ordered as in SVD and a manual selection of the subspace of interest is needed for each channel.

In this paper the proposed method was also compared to PCA for both the simulation study and the analyzed interictal activity (Fig. 2, 4 and 6). In both cases the proposed method performed better than PCA because the latter was not able to segregate the source of interest and the muscle artifact into a separate component. A thorough comparison with other artifact and noise removal techniques described in literature like frequency filtering, adaptive filtering, regression methods and the various ICA algorithms will be the subject of further research. Frequency filtering methods will perform worse in cases where the common activity consists of frequency components that are located in a priori unknown frequency bands. Regression methods and adaptive filter techniques become problematic when a good regressing or noise reference channel is not available as is the case for muscle artifacts. ICA performs well in removing a wide variety of artifacts from EEG records. However, a manual selection of the obtained independent components is required. Moreover, often the muscle artifact appears in nearly all the independent components and even accompanies the ictal component [6].

If one wants to automate the proposed method one must keep in mind that the EDS model becomes ineffective when the signals of interest are not yet started at the onset (n=0) of the selected time window. Consequently, the window length and onset must be chosen adaptively as suggested in [20].

Finally, the method can be applied to other biomedical signals where there is a need to find the common

information within a set of signals (e.g. [21], [22]).

VI. Conclusion

Modelling the common dynamics in multichannel EEG recordings opens new perspectives to removing artifacts and background EEG from interictal and ictal EEG. This paper proposed a subspace based method for modelling the common dynamics which was applied to synthetic data and interictal EEG. In both cases the proposed method removed successfully the artifact and background activity and performed better than PCA. Further research will be required to compare the method with other existing artifact removal methods in order to fully assess the potential and limitations of this new method.

Acknowledgment

The authors would like to thank G. Van Driel for his useful comments in the preparation of the simulation study.

References

[1] E. Niedermeyer, "Epileptic seizure disorder," in *Electroencephalography: Basic Principels, Clinical Applications and Related Fields*, 2nd ed., E. Niedermeyer and F. Lopes da Silva, Eds. Baltimore: Urban and Swarzenberg, 1987, ch. 27.

[2] G. L. Wallstrom, R. E. Kass, A. Miller, J. F. Cohn, and N. A. Fox, "Automatic correction of occular artifacts in the EEG: a comparison of regression-based and component-based methods," *J. Psychophysiol.*, to be published.

[3] Z. J. Koles, J. C. Lind, and A. C. K. Soong, "Spatio-temporal decompositon of the EEG: a general approach to the isolation and localization of sources," *Electroenceph. Clin. Neurophysiol.*, vol. 95, pp. 219–230, Sept. 1995.

[4] T.-P. Jung, S. Makeig, C. Humphries, T.-W. Lee, M. J. McKeown, V. Iragui, and T. J. Sejnowski, "Removing electroencephalographic artifacts by blind source seperation," *Psychophysiology*, vol. 37, pp. 163–178, 2000.

[5] K. Kobayashi, C. J. James, T. Nakahori, T. Akiyama, and J. Gotman, "Isolation of epileptiform discharges from unaveraged EEG by independent component analysis," *Clin. Neurophysiol.*, vol. 110, pp. 1755–1763, 1999.

[6] H. Nam, T.-G. Yim, S. K. Han, J. Oh, and S. K. Lee, "Independent component analysis of ictal EEG in medial temporal lobe epilpesy," *Epilepsia*, vol. 43, no. 2, pp. 160–164, 2002.

[7] C. J. James and J. Gibson, "Temporally constrained ICA: An applicaton to artifact rejection in electromagnetic brain signal analysis," *IEEE Trans. Biomed. Eng.*, vol. 50, no. 9, pp. 1108–1116, Sept. 2003.

[8] J.-M. Papy, L. De Lathauwer, and S. Van Huffel, "A technique for common pole estimation in the multi-channel case," Katholieke Universiteit Leuven, Dept. of Electr. Eng. ESAT-SCD/SISTA, Internal Report 04-70, 2004. [Online]. Available: ftp://www.esat.kuleuven.ac.be/pub/sista/papy/reports/jmp-04-70.ps.gz

[9] J. C. de Munck, H. M. Huizenga, L. J. Waldorp, and R. M. Heethaar, "Estimating stationary dipoles from MEG/EEG data contaminated with spatially and temporally correlated background noise," *IEEE Trans. Signal Processing*, vol. 5, no. 7, pp. 1565–1572, July 2002.

[10] J. G. Proakis and D. G. Manolakis, *Digital Signal Processing*, 3rd ed. Upper Saddle River, New Jersey: Prentice Hall, 1996.

[11] G. H. Golub and W. Kahan, "Calculating the singular values and pseudoinverse of a matrix," *SIAM J. Numer. Anal.*, vol. 2, pp. 205–224, 1965.

[12] G. Golub and C. F. Van Loan, *Matrix computations*, 2nd ed. Baltimore: John Hopkins University Press, 1989.

[13] S. Van Huffel, H. Chen, C. P. Decanniere, and P. Van Hecke, "Algorithm for time-domain NMR data fitting based on total least squares," *J. Magn. Res. A*, vol. 110, pp. 228–237, 1994.

[14] A. J. Cadzow, "Signal enhancement-a composite property mapping algorithm," *IEEE Trans. Acoust., Speech, Signal Processing*, vol. 36, no. 1, pp. 49–62, 1988.

[15] Y. Salu, L. G. Cohen, D. Rose, S. Sato, C. Kufta, and M. Hallet, "An improved method for localizing electric brain dipoles," *IEEE Trans. Biomed. Eng.*, vol. 37, no. 7, pp. 699–708, 1990.

[16] T. F. Oostendorp, J. Delbeke, and D. F. Stegeman, "The conductivity of the human skull: Results of in vivo measurements," *IEEE Trans. Biomed. Eng.*, vol. 47, no. 11, pp. 1487–1492, 2000.

[17] B. N. Cuffin, D. Cohen, K. Ynokuchi, R. Maniewski, C. Purcell, G. R. Cosgrove, J. Ives, J. Kennedy, and D. Schomer, "Tests of EEG localization accuracy using implanted sources in the human brain," *Ann. Neurol.*, vol. 29, pp. 132–138, 1991.

[18] M. R. Nuwer, G. Comi, R. Emmerson, *et al.*, "IFCN standards for digital recording of clinical EEG," *Electroencephalogr Clin Neurophysiol*, vol. 106, pp. 259–261, 1998.

[19] C. J. James and D. Lowe, "Extracting multisource brain activity from a single electromagnetic channel," *Artif. Intell. Med.*, vol. 28, pp. 89–104, 2003.

[20] J. Nieuwenhuijse, R. Heusdens, and E. F. Deprettere, "Robust exponential modeling of audio signals," in *Proc. of International Conference on Acoustic, Speech and Signal Processing (ICASSP 98)*, vol. 6, 1998, pp. 3581–3584.

[21] P. Lemmerling, L. Vanhamme, R. Romano, and S. Van Huffel, "A subspace time-domain algorithm for automated NMR normalization," *J. Magn. Res.*, vol. 157, no. 2, pp. 190–199, Aug. 2002.

[22] G. Morren, S. Van Huffel, I. Helon, G. Naulaers, H. Daniels, H. Devlieger, and P. Caesar, "Effects of non-nutritive sucking on heart rate, respiration and oxygenation: a model-based signal processing approach," *Comp. Biochem. Physiol. A*, vol. 132, pp. 97–106, 2002.

LIST OF FIGURES

1 Simulated data. (a) The time course of the scalp potentials reflecting the 4 Hz epileptiform activity on each electrode. (b) The noise matrix containing awake background EEG, 50 Hz line noise (electrodes O1, P3) and muscle artefact (electrodes F8, Cz). 16
2 (a) The simulation data matrix $L(\lambda)$ for a noise level equal to $nl = 0.95$. (b) The signal matrix A containing the common dynamics. (c) The EEG signals after preprocessing each channel separately. (d) The reconstructed EEG based on the common signal poles. (e) The reconstructed EEG based on the first principal component. 17
3 The singular values of the stacked matrix $U_{stacked}$ generated in the simulation study. 18
4 The RRMSE as a function of the noise level is shown for the proposed method and PCA. . 19
5 10 s epoch of an EEG recorded from a long-term Epilepsy Monitoring unit. The EEG between the dashed lines is selected for further analysis and is shown in fig. 6(a). 20
6 (a) Shows the original spike. The EEG after preprocessing each channel separately is shown in (b). The fit based on the common signal poles is shown in (c). The reconstructed EEG based on the first principal component is shown in (d). 21
7 The singular values of the stacked matrix $U_{stacked}$ generated in the real-life example. 22

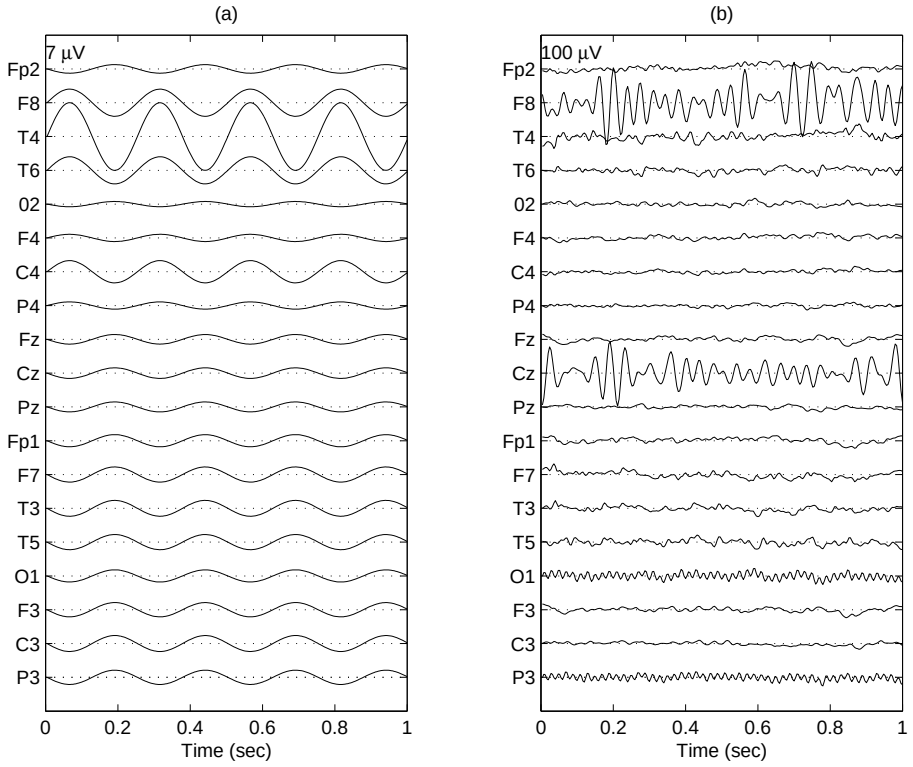


Fig. 1. Simulated data. (a) The time course of the scalp potentials reflecting the 4 Hz epileptiform activity on each electrode. (b) The noise matrix containing awake background EEG, 50 Hz line noise (electrodes O1, P3) and muscle artefact (electrodes F8, Cz).

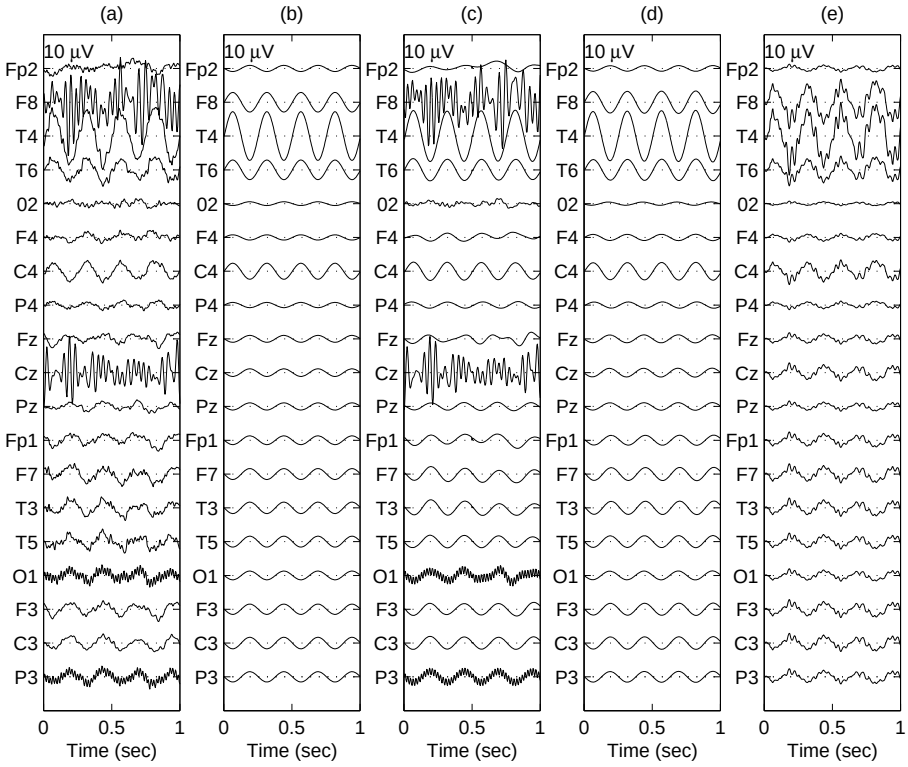


Fig. 2. (a) The simulation data matrix $L(\lambda)$ for a noise level equal to $nl = 0.95$. (b) The signal matrix A containing the common dynamics. (c) The EEG signals after preprocessing each channel separately. (d) The reconstructed EEG based on the common signal poles. (e) The reconstructed EEG based on the first principal component.

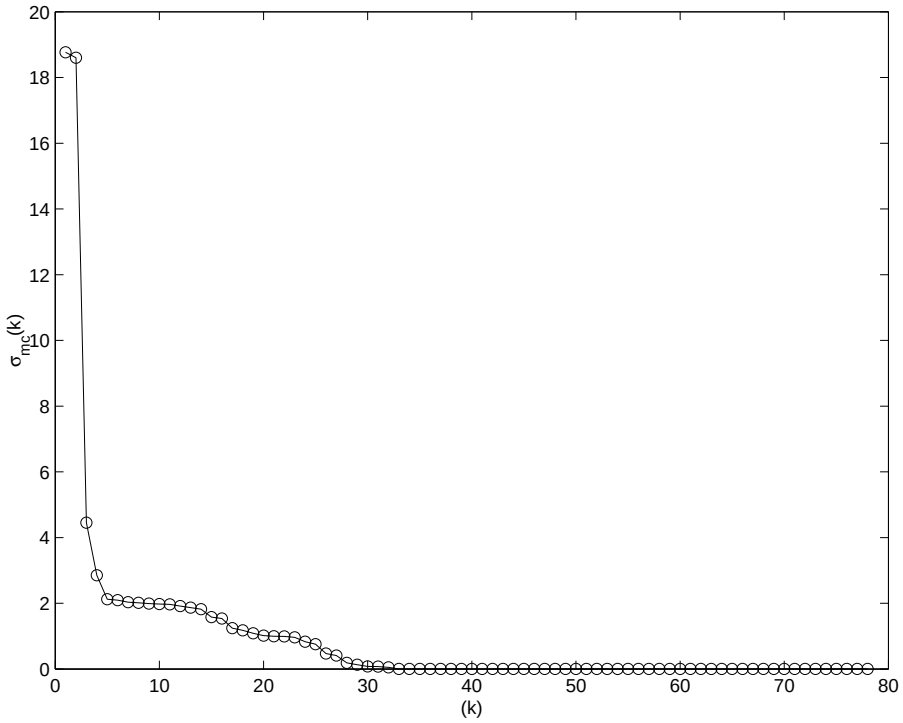


Fig. 3. The singular values of the stacked matrix $U_{stacked}$ generated in the simulation study.

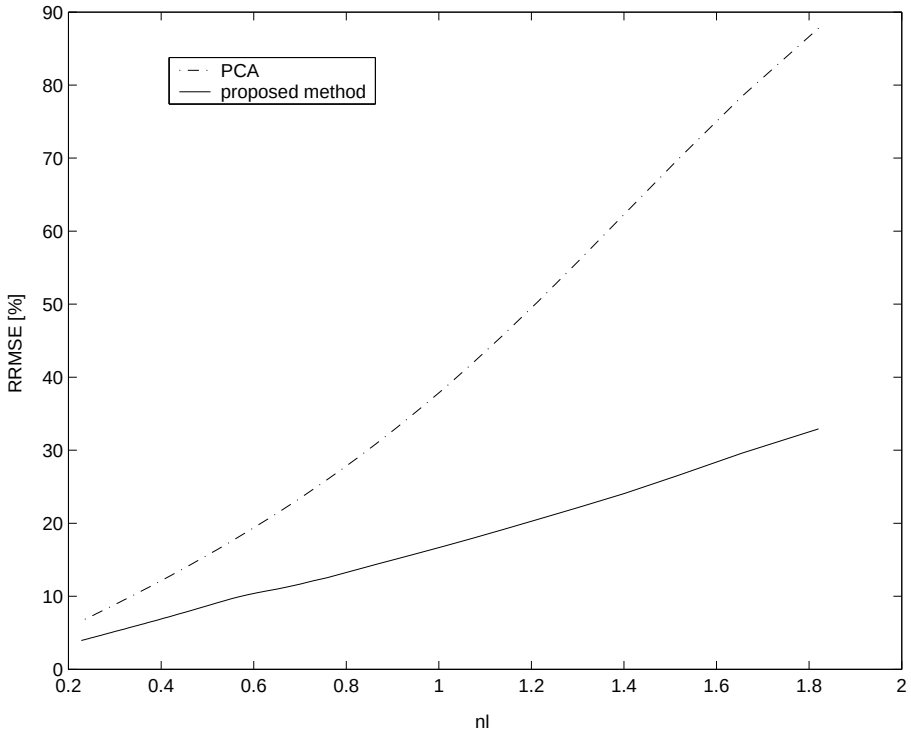


Fig. 4. The RRMSE as a function of the noise level is shown for the proposed method and PCA.

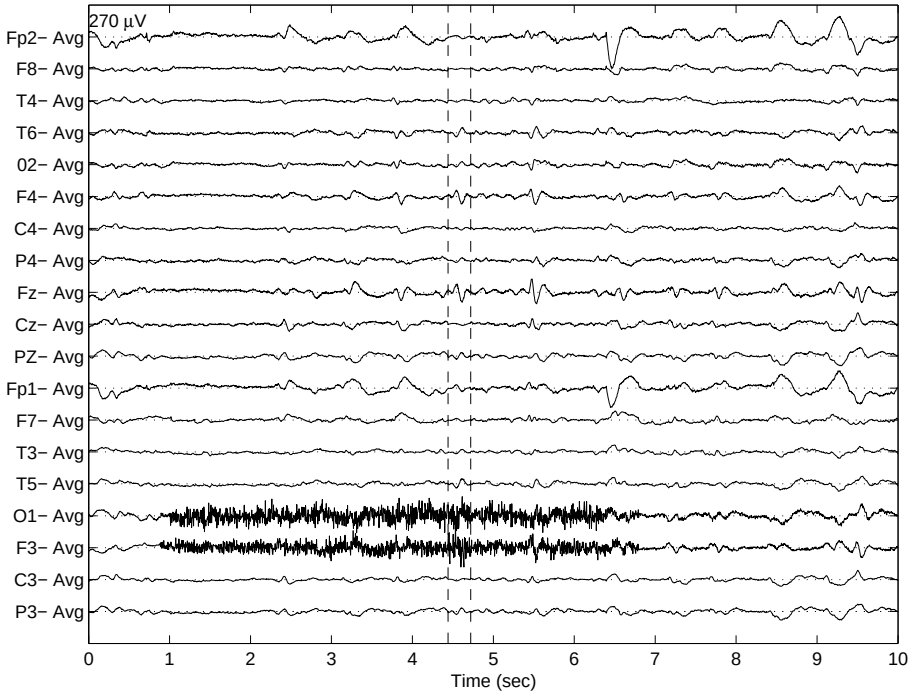


Fig. 5. 10 s epoch of an EEG recorded from a long-term Epilepsy Monitoring unit. The EEG between the dashed lines is selected for further analysis and is shown in fig. 6(a).

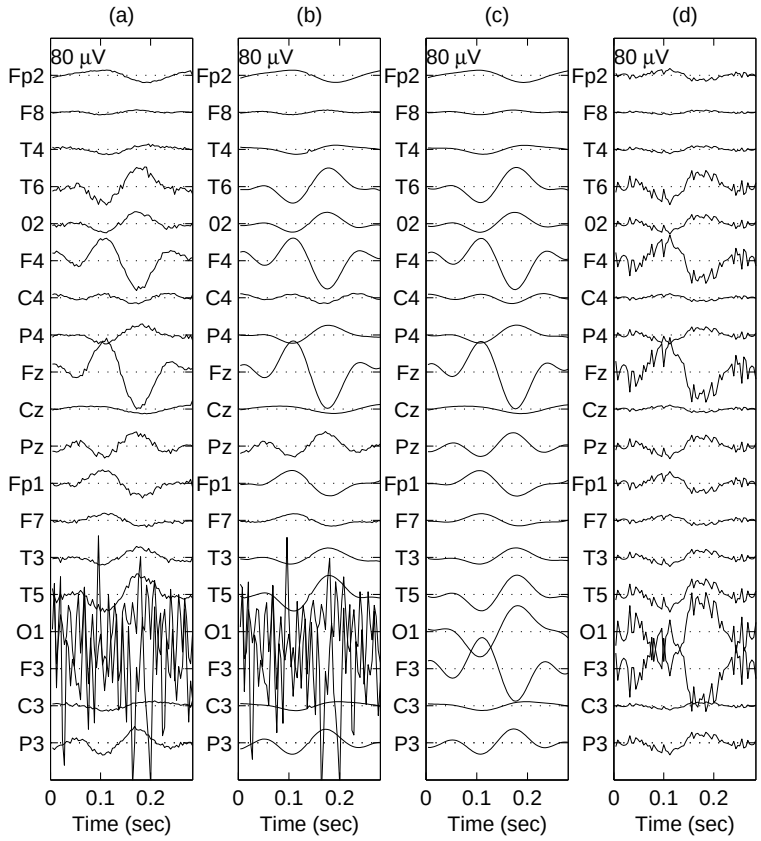


Fig. 6. (a) Shows the original spike. The EEG after preprocessing each channel separately is shown in (b). The fit based on the common signal poles is shown in (c). The reconstructed EEG based on the first principal component is shown in (d).

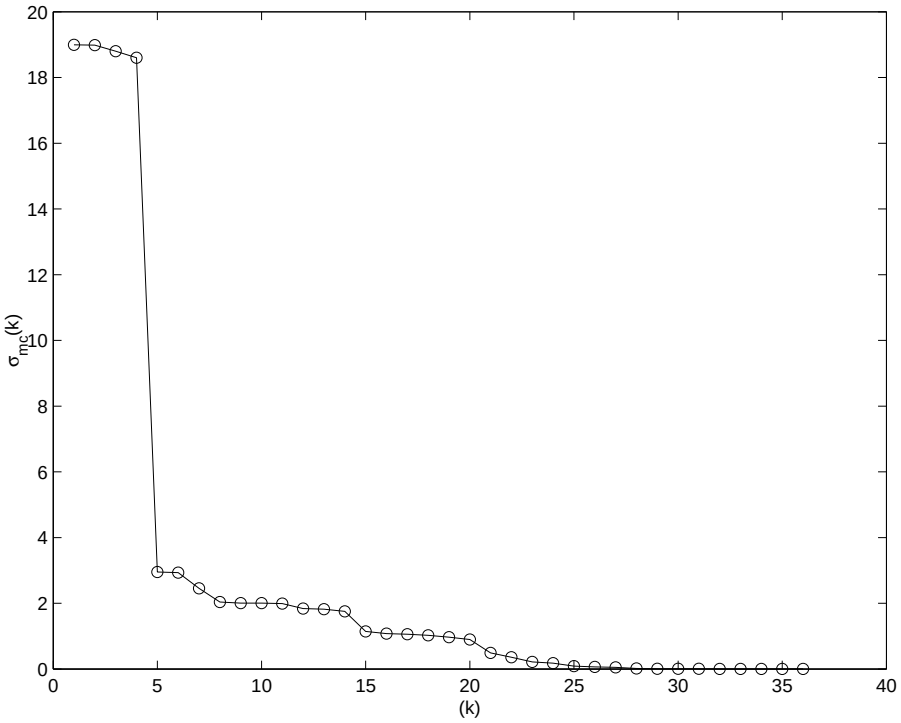


Fig. 7. The singular values of the stacked matrix $U_{stacked}$ generated in the real-life example.